This article has been accepted for publication in a future issue of this journal, but has not been fully edited. Content may change prior to final publication. Citation information: DOI 10.1109/ACCESS.2022.3175847, IEEE Access

IEEE Access
Multidisciplinary | Rapid Review | Open Access Journal

Digital Object Identifier

Sensorless Robust Flatness-Based Control with Nonlinear Observer for Non-Ideal Parallel DC-AC Inverters

AHMED SHAHIN[1] (Senior Member, IEEE), SAYED ABULANWAR[1*] (Member, IEEE), ABDELHADY GHANEM[1] (Member, IEEE), MOHAMMAD E. M. RIZK[1] (Member, IEEE), FUJIN DENG[2] (Senior Member, IEEE), SERGE PIERFEDERICI[3] AND ISLAM ISMAEL[1]

[1]Electrical Engineering Department, Faculty of Engineering, Mansoura University, Mansoura 35516, Egypt.
[2]School of Electrical Engineering, and Jiangsu Key Laboratory of Smart Grid Technology and Equipment, Southeast University, Nanjing 210096, China.
[3]ENSEM-LEMTA-University of Lorraine, 54500, Vandoeuvre-lès-Nancy, France.

Corresponding author: Sayed Abulanwar (e-mail: abulanwar@mans.edu.eg).

ABSTRACT Parallel operation of multiple AC/DC inverters is favorable in hybrid AC/DC microgrids to avert consecutive conversion stages and increase the system's efficacy. Yet, several emerging technical challenges impede the expansion of such layout such as the circulating currents, sensitiveness to the input voltage disturbances, load variations and complexity of the control structures caused by using several required measurements. This paper proposes a one-loop sensorless controller which is based on the flatness technique for a non-isolated power supply consisting of n-parallel inverters. The proposed control scheme primarily relies on employing a nonlinear online observer to estimate the line inductor currents and the dc link voltage via information from the input voltage, output voltage, and load conditions to avoid using excessive sensors. In this way, the system reliability is improved by reducing burdens of the communication delays and/or the failures, signal noise, thus the system is featured by simple control. Besides, the system entire losses are modeled by equivalent voltage sources and one current source which implicitly represent all types of the losses by using an online nonlinear estimator for the control purposes. The proposed controller not only has high dynamic performance, wide-bandwidth, low voltage THD but also robust to the abrupt variations in the load and the input voltage. To validate the applicability of the proposed control method and the observer, both simulations and experimental investigations are performed for two paralleled three-phase inverters setup. The obtained results assure the effectiveness of the proposed control method in regulating the output voltage of the parallel DC/AC inverters with fewer number of the sensors against the fluctuations of the input dc voltage and the load perturbations.

INDEX TERMS Flatness control, losses estimation, parallel inverters, sensorless control, nonlinear observer.

Nomenclature

Acronyms

EKF	Extended Kalman Filter
ESS	Energy storage systems
FBC	Flatness-based controller
FL-VSIs	Four-leg voltage source inverters
PCC	Point of common coupling
PMSM	Permanent magnet synchronous machine
THD	Total harmonic distortion
VSI	Voltage source inverter

Symbols

$*$	Reference value
δ	Fictive control variable
ω	Natural frequency
ϕ	Flat output vector
ψ	Input vector matrix
τ	Time constant
w	Energy vector
w_z	Current error vector
θ	State vector matrix
ε	Error variables of state vector and estimated parameters
φ	State vector matrix

This article has been accepted for publication in a future issue of this journal, but has not been fully edited. Content may change prior to final publication. Citation information: DOI 10.1109/ACCESS.2022.3175847, IEEE Access

ζ	Damping factor
C	Capacitance
G	Nonlinear given function
H	Nonlinear given function
I	Current
k	Dynamics parameter
L	Inductance, load
$Loss$	Losses
n	Paralleled DC-AC inverters
P	Active power
p	Estimated parameters
$p(s)$	Characteristic polynomial
Q	Reactive power
r	Resistance
S	Positive-definite matrix
t	Time
u	Input vector
V	Voltage, Lyapunov function
X	State variable and estimated parameters vector
x	State variable vector

Subscripts

$0dq$	Synchronous Park frame components
wc	Index of characteristic polynomial of energy
wz	Index of characteristic polynomial of current
abc	Three phase quantities
c	Capacitor
dc	DC link
f	Filter
ij	Index of control dynamic parameters of energy; $i = 1:2, j = 1:3$
$initc$	Initial time for reference trajectories of energy
$initz$	Initial time for reference trajectories of current
k	Inverter number index
L	Load
N	Number of total state
n	Total number of inverters
p	Equivalent current source
p, i	Index of estimator parameter
ref	Reference
t	Estimated voltage
x, p	Index of error variables of state vector
x, y	Index of constants of convergence parameters of estimator dynamics
z	Index of circulating current flat output

I. INTRODUCTION

THE recent advance in DC/AC inverters are gaining remarkable attraction in various fields such as the hybrid microgrids (MGs) [1], electric transportation systems, and machine drive applications, owing to their high energy-conversion efficiency that allow it transfer bulk power [2]–[6]. The control structures which are dedicated for parallel DC/AC inverters entail robust performance against variations in the power supply, load, system parameters. Meanwhile, they ensure adequate stability under conceivable operating conditions [7]–[11]. Modern control theories like the FBC necessitates more sensors than the linear controllers such as PI compensators [12], [13]. However, employing many sensors results in increasing the system cost, weight, volume, and complexity of the system. Thus, worsening the reliability, increasing the installation difficulty, increasing the need for proper wiring, and high sensor-breakdown incidence [14], [15]. The sensorless-based control architectures are implemented in diverse power electronic converters such as the boost, buck, three-phase inverters, and full-bridge DC/DC or DC/AC converters [16]–[19]. Accordingly, various strategies are proposed to dispense multiple sensors in the hybrid MGs, power converters, electric machines, and electric transportation. Instead, the observers are used to estimate the state variables and build an accurate model to render the system as sensorless-based control structure [20]–[25]. The sensorless controller which is based on a state observer is employed in [26], [27] for a three-phase inverter by using Lyapunov method. In [25], a current observer is presented to replace the current sensor and estimate the inductor current despite disturbances and uncertainties. This observer can estimate the transformer current in a full-bridge isolated converter. This method is based on the transient dc bias characterization and the load current feedforward. However, these approaches rely on complicated computations which need a high speed controller with high processing capability. Therefore, emerging delays and complicated control system leading to inadvertent performance issues and thus, the DC link voltage transient oscillations can't be completely mitigated using this method.

In [26], a Lyapunov-based control is also used to eliminate the observer error under the load changes and uncertainty conditions. Where many computational vectors are handled every sampling step for the real time control and high capability of a digital processor is needed.

In [28], the flatness theory is employed to ascertain efficient performance of the FL-VSIs under different loading conditions. The application of the flatness control enhances the PMSM drive performance as a model-based estimation [29]. The flatness controllers ensure that, the state variables can accurately follow a prescribed behavior either during normal or transient conditions for the AC/DC systems. Besides, the flatness technique is robust against the changes in the system parameters and the load conditions, thus the flatness control allows high communication among the units [30].

Therefore, the flatness-based control approach is preferable for the nonlinear controllers which are devoted to the control of the parallel DC/AC inverters [31]. For example, in [30], [32] the flatness control is implemented to the paralleled VSIs to achieve reliable operation during the normal as well as abnormal scenarios due to sudden loss of any inverter. On the other hand, the flatness techniques planning features which are based on ESSs are investigated in [33]–[36]. The choice of one loop control structure which is based on the flatness guarantees higher bandwidth controller, low noise, lower output voltage THD and better damped transient performance [30], [32]–[36]. Moreover, the inher-

This article has been accepted for publication in a future issue of this journal, but has not been fully edited. Content may change prior to final publication. Citation information: DOI 10.1109/ACCESS.2022.3175847, IEEE Access

ent system enables estimating the state variables behavior without integration, by the instant conduct of the controlled flat output. The FBC for parallel DC/AC inverters is realized in a master-slave manner where, the first inverter performs as a master dictating the output voltage whereas, the other inverters behave as slave, where, either output currents or load power is adjusted between the parallel inverters. The control schemes which are based on master-slave are extensively employed to share the load power, suppress circulating currents and enhancing the system reliability [37], [38]. This paper suggests a one-loop FBC for a non-isolated power supply composed of n-parallel DC/AC inverters. Additionally, an online observer is augmented to estimate the inductor line currents and the dc link voltage via the information from the input voltage, output voltage, and load conditions. In this manner, the number of the sensors that are used in the FBC is minimized to overcome the complexity of the control structure, signal noise and potential communication failures and/or delays. Table 1 compares the FBC to other typical control structures which are usually dedicated for DC/DC and/or DC/AC converters. The comparison shows that the FBC demonstrates high dynamic performance compared to the other existing control techniques. Moreover, the FBC provides a good tracking performance, robustness to the parameters variation, high capability for disturbance rejection, and easy for the implementation in the real time [39]. Furthermore, due to its superior properties, the FBC can be integrated with conventional PI controllers. A loop-shaping problem is formulated where a combination of FBC with PI regulator is incorporated with the control system [40]. With the FBC, the measured trajectory is planned to follow a predefined reference trajectory with a high grade of accuracy and reliability. Accordingly, owing to its high dynamic performance, the FBC responds quickly in case of abrupt load changes which makes it also preferable to assist in the fault-tolerant control design of the power electronic converters, such as the open-switch faults [32].

Major contributions of this paper are:
(1) Using FBC scheme to not only regulate output voltage of the parallel inverters but also increase system robustness against abrupt variations of supply voltage and load. The FBC properties would enhance reliability of the parallel inverters operation in any conceivable application such as that in hybrid AC/DC MGs. (2) A nonlinear observer is suggested to minimize the number of required sensors in the entire system in order to simplify the control scheme and counteract controller sensitivity to noise of measured signals and/or failures. (3) Proposed losses estimation approach for the DC/AC inverters is augmented to estimate the entire system losses by equivalent voltage sources and one current source..

II. SYSTEM STRUCTURE AND ANALYSIS

The layout of a typical n-parallel three-phase DC/AC inverters is illustrated in Fig. 1. To estimate the losses of the parallel inverters system, three serial equivalent voltage sources V_{tabcn} and current source I_P at the input dc-link are employed. During the balanced conditions, sum of the load side currents is zero, as in (1). Likewise, sum of the inverter output line currents is zero at the PCC, as given by (2).

$$i_{La} + i_{Lb} + i_{Lc} = 0 \tag{1}$$

$$\sum_{k=1}^{n} i_{ak} + i_{bk} + i_{ck} = 0 \tag{2}$$

Consequently, sum of i_{cabcs} is zero and sum of V_{cabcs} is constant. Then, the system has $3n + 5$ variables and two special linked relations. The derivative of the voltages V_{cdq} at the PCC with $V_{co} = 0$ are defined as:

$$\begin{pmatrix} \dot{V}_{cd} \\ \dot{V}_{cq} \end{pmatrix} = \begin{pmatrix} 0 & \omega \\ -\omega & 0 \end{pmatrix} \begin{pmatrix} V_{cd} \\ V_{cq} \end{pmatrix} + \frac{1}{C_f} \left(\begin{pmatrix} \sum_{k=1}^{n} i_{dk} \\ \sum_{k=1}^{n} i_{qk} \end{pmatrix} - \begin{pmatrix} i_{Ld} \\ i_{Lq} \end{pmatrix} \right) \tag{3}$$

According to Fig. 1, and as implied from (2), sum of the homopolar currents at the PCC is zero i.e., $\sum_{k=1}^{n} i_{0k} = 0$. Thus, the current state variables are of the order $n - 1$. Arbitrarily, the homopolar current of the first inverter (the master one), can be found as $i_{01} = -\sum_{k=1}^{n} i_{0k}$ (any another inverter can be behave as master). Consequently, the homopolar currents of the remaining $(n-1)$ inverters become independent variables. Then, the master inverter output line current dq components can be formulated as:

$$\begin{pmatrix} \dot{i}_{d1} \\ \dot{i}_{q1} \end{pmatrix} = \begin{pmatrix} -\frac{r_1}{L_1} & \omega \\ -\omega & -\frac{r_1}{L_1} \end{pmatrix} \begin{pmatrix} i_{d1} \\ i_{q1} \end{pmatrix} + \frac{1}{L_1} \left(\begin{pmatrix} V_{d1} \\ V_{q1} \end{pmatrix} - \begin{pmatrix} V_{td1} \\ V_{tq1} \end{pmatrix} - \begin{pmatrix} V_{cd} \\ V_{cq} \end{pmatrix} \right) \tag{4}$$

The inductive currents of any k^{th} module, with $k \in [2, .., n]$ can be written as:

$$\begin{pmatrix} \dot{i}_{0k} \\ \dot{i}_{dk} \\ \dot{i}_{qk} \end{pmatrix} = \begin{pmatrix} -\frac{r_k}{L_k} & 0 & 0 \\ 0 & -\frac{r_k}{L_k} & \omega \\ 0 & -\omega & -\frac{r_k}{L_k} \end{pmatrix} \begin{pmatrix} i_{0k} \\ i_{dk} \\ i_{qk} \end{pmatrix} + \frac{1}{L_k} \left(\begin{pmatrix} V_{0k} \\ V_{dk} \\ V_{qk} \end{pmatrix} - \begin{pmatrix} V_{t0k} \\ V_{tdk} \\ V_{tqk} \end{pmatrix} - \begin{pmatrix} V_{c0} \\ V_{cd} \\ V_{cq} \end{pmatrix} \right) \tag{5}$$

Voltages $V_{t0k}, V_{tdk}, V_{q0k}$ for $k \in 1, .., n$ represent the voltages drops through the system which result from the losses. In this model, the parameters V_{tdqk}, indirectly represent the losses through the entire system, and as these parameters vary slowly, their time-derivatives are neglected. The dynamics of the DC link can be described as:

$$V_{in} = L\frac{di}{dt} + r_L i_L + V_{dc} \tag{6}$$

This article has been accepted for publication in a future issue of this journal, but has not been fully edited. Content may change prior to final publication. Citation information: DOI 10.1109/ACCESS.2022.3175847, IEEE Access

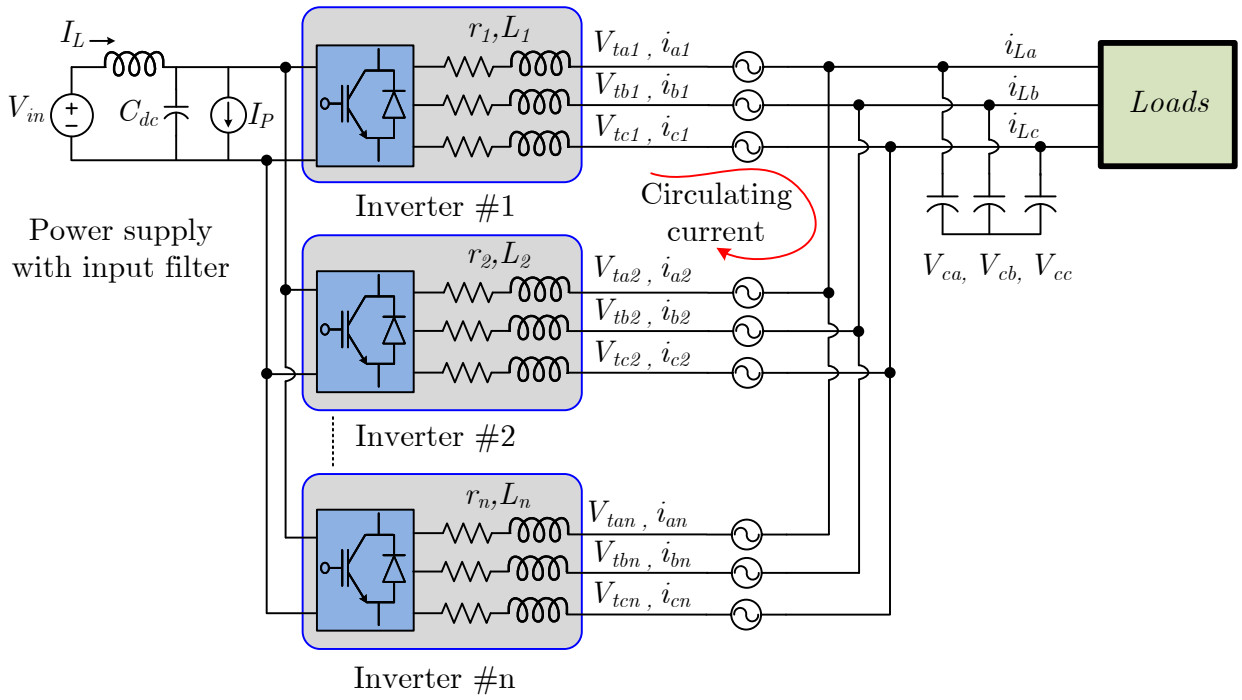

FIGURE 1: The system of n parallel DC/AC inverters.

TABLE 1: Comparison between FBC with other control methods

Parameter of Comparison	PID Control	Sliding Mode Control	Fuzzy Logic Control	Flatness Control
Type of control	Linear	nonlinear	Artificial intelligent	Nonlinear
Control suitability	Low-order system	All types of systems	All type of system	All types of systems
Accurate mathematical modeling	Needed	Needed	Not needed	Needed to prove the system is flat
Analogue/digital control	Yes/yes	Yes/yes	No/yes	Yes/yes
Requirements of current sensing	No	Yes	May or may not be	no
Sensitivity to parameters and load changes	Sensitive	Insensitive	Insensitive	Insensitive
Overshoot	Large	Negligible	Negligible	Negligible
Large signal dynamics consistency	Average	Good	Excellent	Excellent
Ease of handling complex system	Complex	Easy	Very Easy	Very easy
Control complexity	Medium	higher	Low	low

$$C_{dc}\frac{dV_{dc}}{dt} = i_L - I_P - \frac{1}{V_{dc}}\sum_{k=1}^{n}(V_{dk}i_{dk} + V_{qk}i_{qk}) \quad (7)$$

III. OBSERVABILITY AND ESTIMATOR

A. PARAMETER OBSERVABILITY OF NONLINEAR SYSTEM

There are several ways to prove the observability of a system where observability conditions and methods are discussed in [41]–[47]. The observability of the estimated parameters V_{tdq} and I_p must be verified before the derivatives of the estimator. By proving the observability of the system, the estimated variables exponentially converge to the real ones with the proposed state observer. The proposed state observer is inspired from the subclass of the state observers which is designated in [48], [49]. The considered state vector $X = [x, p]^T$ where p represents the estimated parameters as detailed later, is given as follows:

$$X = \Big[x, p\Big]^T \quad (8)$$

$$\begin{cases} x = [i_{dq0n}\ V_{cdq}\ V_{dc}\ I_{dc}]^T \\ p = [V_{tdqn}\ I_p]^T \end{cases} \quad (9)$$

The measured state variables y (in our case y=x) is given by:

This article has been accepted for publication in a future issue of this journal, but has not been fully edited. Content may change prior to final publication. Citation information: DOI 10.1109/ACCESS.2022.3175847, IEEE Access

$$y = x = [i_{dq0n}\ V_{cdq}\ V_{dc}\ I_{dc}]^T \tag{10}$$

The observability vector θ of such system can be considered as following:

$$\theta = \begin{pmatrix} y \\ \dot{y} \end{pmatrix} \tag{11}$$

According to the criterion in [48], [49]

$$rank(Jacob(\theta)) = dim(X) = 13 \tag{12}$$

For the proposed system, there are three currents for each inverter and two voltage values for the ac bus. In addition, one current source I_p, and two voltages V_{tdq} to be estimated, besides the input variables V_{dc} and I_{dc}. For the given system, two inverters in parallel are considered ($n = 2$), it can be easily proved that rank $(Jacob(\theta)) = 13$. Thus, in the considered case, the system is observable.

B. DEFINITION OF PROPOSED STATE-OBSERVER

In this section, a state observer is proposed. This observer is applied to a specific subclass of nonlinear systems which is based on nonlinear FBC. The state variables are required to estimate the system parameters to obtain the differential flatness property. The losses through the whole system are estimated and modelled which are considered as a disturbance which is compared to the ideal system. The estimated parameters are linked to the state variables of the model. Then, an online state observer (or parameter estimator) is essential to enhance the system performance.

Several observation techniques exist in the literature, contrary to the Extended Kalman Filter (EKF) or Luenberger observers, a thorough comparison bethween the EKF and Luenberger observers is elaborated in [48]. The proposed observer is well-adapted to the nonlinear systems to estimate the line currents of each inverter and to estimate the unknown parameters V_{tdqk} and I_p. The parallel inverters model can be represented by (13) where x represents the state vector (all variables are supposed to be measured), p is the vector of the unknown parameters whose dynamics are too slow. So, they are considered as constant in the steady state. The differential system which is used to estimate these parameters can be firstly described as:

$$\dot{x} = \begin{pmatrix} \dot{x} \\ \dot{p} \end{pmatrix} = G(x) + H(x,u)p \tag{13}$$

where the two functions G, H are nonlinear and u is the input vector. The estimated state variables, parameters, and their dynamics are given by:

$$\dot{\hat{x}} = G(x) + H(x,u)\hat{p} - S(\hat{x} - x) \tag{14}$$

$$\dot{\hat{p}} = k_p(\dot{\hat{x}} - \dot{x}) + \left(k_i - H(x,u)^T\right)(\hat{x} - x) \tag{15}$$

for $n = 2$ and identical filter line inductances, the system becomes:

$$\begin{cases} \hat{x} = [\hat{i}_{dq0n}\ \hat{V}_{cdq}\ \hat{V}_{dc}\ \hat{I}_{dc}]^T \\ \hat{p} = [\hat{V}_{tdqn}\ \hat{I}_P]^T \end{cases} \tag{16}$$

$$G = \begin{bmatrix} -\frac{r_k}{L_k} & 0 & 0 \\ 0 & -\frac{r_k}{L_k} & \omega \\ 0 & -\omega & -\frac{r_k}{L_k} \end{bmatrix},$$

$$H = \begin{bmatrix} -\frac{1}{L_f} & 0 & 0 & 0 & 0 \\ 0 & -\frac{1}{L_f} & 0 & 0 & 0 \\ 0 & 0 & -\frac{1}{L_f} & 0 & 0 \\ 0 & 0 & 0 & -\frac{1}{L_f} & 0 \\ 0 & 0 & 0 & 0 & 0 \\ 0 & 0 & 0 & 0 & 0 \\ 0 & 0 & 0 & 0 & -\frac{1}{C_{dc}} \end{bmatrix} \tag{17}$$

where $\hat{x} \in R^{2n+4}$ and $\hat{p} \in R^{2n+1}$. $S \in R^{(2n+4)(2n+4)}$ a positive definite matrix. The estimator dynamic parameters are given by:

$$k_p \cdot H(x,u) = -S$$

$$k_i = k_p S$$

Determining of parameters k_p and k_i depends on inverse of the matrix $H(x,u)$, where H is not square. Parameter k_p (consequently k_i) is calculated by considering a pseudoinverse of $H(x,u)$.

The following error variables are introduced:

$$\begin{cases} \epsilon_x = \hat{x} - x \\ \epsilon_p = \hat{p} - p \end{cases} \tag{18}$$

where $\dot{p} = 0$. The proposed observer is expressed by:

$$\dot{\epsilon}_x = H(x,u) \cdot \epsilon_p - S \cdot \epsilon_x \tag{19}$$

$$\dot{\epsilon}_p = k_p \cdot \dot{\epsilon}_p + \left(k_i - H(x,u)^T\right) \cdot \epsilon_x \tag{20}$$

C. ESTIMATION STABILITY VERIFICATION

To validate the stability of the suggested estimator, a candidate Lyapunov function is selected. The exponential stability can be readily verified via classical Lyapunov method. Accordingly, the proposed estimator stability and dynamics are dictated by coefficients k_i and H as given by (19) and (20). Hence, to explore their stability, the candidate Lyapunov function is expressed by:

$$V = \frac{1}{2}\left(\epsilon_x^T \epsilon_x + \epsilon_p^T \epsilon_p\right) \tag{21}$$

This function is globally positive-definite over the whole state space. The time-derivative of (21) is defined as:

$$\dot{V} = \frac{1}{2}\left(\dot{\epsilon}_x^T \epsilon_x + \dot{\epsilon}_p \epsilon_p^T\right) \tag{22}$$

This article has been accepted for publication in a future issue of this journal, but has not been fully edited. Content may change prior to final publication. Citation information: DOI 10.1109/ACCESS.2022.3175847, IEEE Access

Assuming $\hat{x} = x$, so, the system dynamics is slow. By substitute from (19) and (20) into (22), the derivative of V become as following:

$$\begin{cases} \dot{V} = \left(\epsilon_x^T \dot{\epsilon}_x + \epsilon_p^T \dot{\epsilon}_p\right) = \epsilon_x^T \Big(H(x,u)\epsilon_p - S\epsilon_x\Big) \\ \qquad\qquad + \epsilon_p^T \Big(k_p \dot{\epsilon}_x + (k_i - H(x,u)\epsilon_x)\Big) \end{cases} \tag{23}$$

The exponential stability of the estimator can be guaranteed since S is a positive-definite matrix. The tuning of the S matrix is determined to ensure that, the dynamics of ϵ_x quite faster than that of ϵ_p. Then, by employing the value of $kp.H(x,u) = -S$ and $k_i = k_p.S$, it results in:

$$\dot{V} \leq -V \tag{24}$$

The candidate Lyapunov function demonstrated that the estimation errors exponentially converge to zero, then, the system is exponentially stable.

IV. PROPOSED CONTROL SCHEME

A. IMPLEMENTATION OF CONTROLLER BASED ON FLATNESS THEORY

Differential flat systems are a specific class of the control systems. Under this control system, the structure of the desired trajectories and their dynamics can be completely characterized, Martin *et. al* [31]. Accordingly, all state and input variables can be expressed in terms of a set of particular variables (i.e., the flat outputs) and their derivatives. More specifically, a system with a state vector $x \in R^n$, and input vector $u \in R^m$, is termed differentially flat if x and u can be found as a function of the chosen flat output $\mathrm{w} \in R^m$ (the number of input variables equals the number of the flat outputs) as the following form:

$$\begin{cases} x = \varphi\Big(\mathrm{w}, \dot{\mathrm{w}}, .., \mathrm{w}^{(d)}\Big) \\ u = \psi\Big(\mathrm{w}, \dot{\mathrm{w}}, .., \mathrm{w}^{(d+1)}\Big) \\ \mathrm{w} = \phi\Big(x, u, \dot{u}, .., u^{(f)}\Big) \end{cases} \tag{25}$$

where the rank of $(\varphi) = n$, $(\psi) = m$ and $(\phi) = m$.

Thanks to the FBC approach, the prediction of the state variables behavior in both steady-state and transient conditions is feasible. The FBC can planify the trajectory of the flat output and its derivatives [30].

B. APPLICATION OF FBC

Finding a candidate flat output as well as input and state vectors as a function of the candidate flat output without solving the differential equations system is challenging for optimal FBC design.

To realize the control objectives of the proposed parallel inverters system, the energy of the capacitive ac bus and the errors of the circulating currents are picked as the candidate flat outputs. According to the control objectives, the candidate flat outputs vector is selected as the electrostatic energy w_c which is stored in the output ac filtering capacitance and the error of the circulating currents w_{zk} between the parallel inverters. The flat output vector becomes $\mathrm{w} = [\mathrm{w}_c, \mathrm{w}_{zk}]^T$, where $\mathrm{w}_c = [\mathrm{w}_d, \mathrm{w}_q]^T$. The control of w_c to its respective reference w_{c-ref} ascertains voltage constancy of the ac capacitive bus at the PCC, where w_c is defined by (26). The voltage vector $[V_{cd}, V_{cq}]^T$ of the ac capacitance can be rewritten as given by (27).

$$\mathrm{w}_c = \begin{pmatrix} \mathrm{w}_d \\ \mathrm{w}_q \end{pmatrix} = \frac{C_f}{2} \begin{pmatrix} sign(V_{cd})(V_{cd}^2) \\ sign(V_{cq})(V_{cq}^2) \end{pmatrix} = \phi_{\mathrm{w}_c}(x) \tag{26}$$

$$\begin{pmatrix} V_{cd} \\ V_{cq} \end{pmatrix} = \begin{pmatrix} sign(\mathrm{w}_d)\sqrt{2\mathrm{w}_d/C_f} \\ sign(\mathrm{w}_q)\sqrt{2\mathrm{w}_q/C_f} \end{pmatrix} = \begin{pmatrix} \psi_{V_{cd}}(\mathrm{w}_d) \\ \psi_{V_{cq}}(\mathrm{w}_q) \end{pmatrix} \tag{27}$$

The flat output components $\mathrm{w}_{zk} = [\mathrm{w}_{z2}, \ldots, \mathrm{w}_{zn}]^T$ represent the errors of the circulating currents. Each component of w_{zk} allows reducing the circulating currents between the first/master inverter and the k^{th} inverter, with $\mathrm{w}_{zk} \in R^3 \quad \forall \quad k \in \{2, .., n\}$.

Controlling w_{zk} to accurately follow its respective reference w_{zk-ref} ensures not only, that the circulating currents between the parallel inverters are minimized but also, equal distribution of the demanded power among the parallel units. For this purpose, the homopolar currents of $(n-1)$ modules are controlled to cancel the zero-sequence current-component of the first/master inverter homopolar current (i_{01}).

$$\mathrm{w}_{zk} = \begin{pmatrix} \mathrm{w}_{zok} \\ \mathrm{w}_{zdk} \\ \mathrm{w}_{zqk} \end{pmatrix}^T = \begin{pmatrix} z_{ok} \\ z_{dk} \\ z_{qk} \end{pmatrix}^T = \begin{pmatrix} i_{0k} \\ i_{d1} - i_{dk} \\ i_{q1} - i_{qk} \end{pmatrix}^T = \phi_{\mathrm{w}_{zk}}(x) \tag{28}$$

Derivatives of the voltage vector $[V_{cd}, V_{cq}]^T$ and line currents $[i_{d1}, i_{q1}]^T$ are given in terms of w_c, w_{zk} and their respective derivatives by (26), (27) and (28) as following:

$$\begin{pmatrix} \dot{V}_{cd} \\ \dot{V}_{cq} \end{pmatrix} = \begin{pmatrix} 0 & \omega \\ -\omega & 0 \end{pmatrix} \begin{pmatrix} \varphi_{V_{cd}}(\mathrm{w}_d) \\ \varphi_{V_{cq}}(\mathrm{w}_q) \end{pmatrix} + \frac{1}{C_f} \left(\begin{pmatrix} \sum_{k=1}^n i_{dk} \\ \sum_{k=1}^n i_{qk} \end{pmatrix} - \begin{pmatrix} i_{Ld} \\ i_{Lq} \end{pmatrix} \right) \tag{29}$$

$$\begin{pmatrix} i_{d1} \\ i_{q1} \end{pmatrix} = \frac{1}{n} \begin{pmatrix} sign(\mathrm{w}_d)\dot{\mathrm{w}}_d/\sqrt{2\mathrm{w}_d/C_f} + \sum_{j=2}^n Z_{dj} + i_{Ld} \\ sign(\mathrm{w}_q)\dot{\mathrm{w}}_q/\sqrt{2\mathrm{w}_q/C_f} + \sum_{j=2}^n Z_{qj} + i_{Lq} \end{pmatrix} - \begin{pmatrix} 0 & \frac{\omega C_f}{n} \\ -\frac{\omega C_f}{n} & 0 \end{pmatrix} \begin{pmatrix} sign(\mathrm{w}_d)\sqrt{2\mathrm{w}_d/C_f} \\ sign(\mathrm{w}_q)\sqrt{2\mathrm{w}_q/C_f} \end{pmatrix} = \begin{pmatrix} \varphi_{i_{d1}}(\mathrm{w}_c, \dot{\mathrm{w}}_c, \mathrm{w}_z) \\ \varphi_{i_{q1}}(\mathrm{w}_c, \dot{\mathrm{w}}_c, \mathrm{w}_z) \end{pmatrix} \tag{30}$$

The line current i_{0dqk}: $k \in \{2, ..., n\}$ of the remnant k^{th} inverters which is given by using (28) is:

This article has been accepted for publication in a future issue of this journal, but has not been fully edited. Content may change prior to final publication. Citation information: DOI 10.1109/ACCESS.2022.3175847, IEEE Access

$$\begin{pmatrix} i_{0k} \\ i_{dk} \\ i_{qk} \end{pmatrix} = \begin{pmatrix} z_{0k} \\ \varphi_{id1}(\mathrm{w}_c, \dot{\mathrm{w}}_c, \mathrm{w}_z) - z_{dk} \\ \varphi_{iq1}(\mathrm{w}_c, \dot{\mathrm{w}}_c, \mathrm{w}_z) - z_{qk} \end{pmatrix} = \begin{pmatrix} \varphi_{i0k}(\mathrm{w}_z) \\ \varphi_{idk}(\mathrm{w}_c, \dot{\mathrm{w}}_c, \mathrm{w}_z) \\ \varphi_{iqk}(\mathrm{w}_c, \dot{\mathrm{w}}_c, \mathrm{w}_z) \end{pmatrix} \quad (31)$$

The current vector vector is expressed as a function of $\mathrm{w}_c = [\mathrm{w}_d, \mathrm{w}_q]^T$ which is given by (26) and derivatives of the components of the voltage vector $[V_{cd}, V_{cq}]^T$ which are given by (29). Derivatives of dq current components which is given by (30) becomes:

$$\begin{pmatrix} \dot{i}_{d1} \\ \dot{i}_{q1} \end{pmatrix} = \frac{1}{n} \begin{pmatrix} \frac{sign(\mathrm{w}_d)\ddot{\mathrm{w}}_d}{V_{cd}} - \frac{sign(\mathrm{w}_d)\dot{\mathrm{w}}_d}{C_f V_{cd}^2}\left(i_{d1} - i_{Ld} + \omega C_f V_{cq}\right) + \sum_{j=2}^{n} \dot{Z}_{dj} + \dot{i}_{Ld} \\ \frac{sign(\mathrm{w}_q)\ddot{\mathrm{w}}_q}{V_{cq}} - \frac{sign(\mathrm{w}_q)\dot{\mathrm{w}}_q}{C_f V_{cq}^2}\left(i_{q1} - i_{Lq} - \omega C_f V_{cd}\right) + \sum_{j=2}^{n} \dot{Z}_{qj} + \dot{i}_{Lq} \end{pmatrix} - \begin{pmatrix} 0 & \omega/n \\ -\omega/n & 0 \end{pmatrix} \begin{pmatrix} i_{d1} - i_{Ld} + \omega C_f V_{cq} \\ i_{q1} - i_{Lq} - \omega C_f V_{cd} \end{pmatrix} = \begin{pmatrix} \varphi_{di_{d1}}(\mathrm{w}_c, \dot{\mathrm{w}}_c, \ddot{\mathrm{w}}_c, \mathrm{w}_z, \dot{\mathrm{w}}_z) \\ \varphi_{di_{q1}}(\mathrm{w}_c, \dot{\mathrm{w}}_c, \ddot{\mathrm{w}}_c, \mathrm{w}_z, \dot{\mathrm{w}}_z) \end{pmatrix} \quad (32)$$

For the other $(n-1)^{th}$ inverters, derivatives of the inverter output line currents are reformed by (33). Based on the above model, the input/control vector of the master inverter is given by (34).

$$\begin{pmatrix} \dot{i}_{0k} \\ \dot{i}_{dk} \\ \dot{i}_{qk} \end{pmatrix} = \begin{pmatrix} \dot{z}_{0k} \\ \varphi_{di_{d1}}(\mathrm{w}_c, \dot{\mathrm{w}}_c, \ddot{\mathrm{w}}_c, \mathrm{w}_z, \dot{\mathrm{w}}_z) - \dot{z}_{dk} \\ \varphi_{di_{q1}}(\mathrm{w}_c, \dot{\mathrm{w}}_c, \ddot{\mathrm{w}}_c, \mathrm{w}_z, \dot{\mathrm{w}}_z) - \dot{z}_{qk} \end{pmatrix} = \begin{pmatrix} \varphi_{di_{0k}} \dot{w}_z \\ \varphi_{di_{d1}}(\mathrm{w}_c, \dot{\mathrm{w}}_c, \ddot{\mathrm{w}}_c, \mathrm{w}_z, \dot{\mathrm{w}}_z) \\ \varphi_{di_{q1}}(\mathrm{w}_c, \dot{\mathrm{w}}_c, \ddot{\mathrm{w}}_c, \mathrm{w}_z, \dot{\mathrm{w}}_z) \end{pmatrix} \quad (33)$$

$$\begin{pmatrix} V_{d1} \\ V_{q1} \end{pmatrix} = L_1 \begin{pmatrix} \varphi di_{d1} \\ \varphi di_{d1} \end{pmatrix} - L_1 \begin{pmatrix} -\frac{r_1}{L_1} & \omega \\ -\omega & -\frac{r_1}{L_1} \end{pmatrix} \begin{pmatrix} \varphi i_{d1} \\ \varphi i_{q1} \end{pmatrix} + \begin{pmatrix} V_{tdk} \\ V_{tqk} \end{pmatrix} + \begin{pmatrix} \varphi V_{cd} \\ \varphi V_{cq} \end{pmatrix} = \begin{pmatrix} \psi_{V_{d1}}(\mathrm{w}_c, \dot{\mathrm{w}}_c, \ddot{\mathrm{w}}_c, \mathrm{w}_z, \dot{\mathrm{w}}_z) \\ \psi V_{q1}(\mathrm{w}_c, \dot{\mathrm{w}}_c, \ddot{\mathrm{w}}_c, \mathrm{w}_z, \dot{\mathrm{w}}_z) \end{pmatrix} \quad (34)$$

The input/control vector of the $(n-1)^{th}$ inverters can be rewritten as following:

$$\begin{pmatrix} V_{0k} \\ V_{dk} \\ V_{qk} \end{pmatrix} = L_k \begin{pmatrix} \varphi_{di_{0k}} \\ \varphi_{di_{dk}} \\ \varphi_{di_{qk}} \end{pmatrix} - L_k \begin{pmatrix} -\frac{r_k}{L_k} & 0 & 0 \\ 0 & -\frac{r_k}{L_k} & \omega \\ 0 & -\omega & -\frac{r_k}{L_k} \end{pmatrix} \begin{pmatrix} \varphi_{i_{0k}} \\ \varphi_{i_{dk}} \\ \varphi_{i_{qk}} \end{pmatrix} + \begin{pmatrix} V_{t0k} \\ V_{tdk} \\ V_{tqk} \end{pmatrix} + \begin{pmatrix} V_{c0k} \\ \varphi_{V_{cd}} \\ \varphi_{V_{cq}} \end{pmatrix} = \begin{pmatrix} \psi_{V_{0k}}(\mathrm{w}_z, \dot{\mathrm{w}}_z) \\ \psi_{V_{dk}}(\mathrm{w}_c, \dot{\mathrm{w}}_c, \ddot{\mathrm{w}}_c, \mathrm{w}_z, \dot{\mathrm{w}}_z) \\ \psi_{V_{qk}}(\mathrm{w}_c, \dot{\mathrm{w}}_c, \ddot{\mathrm{w}}_c, \mathrm{w}_z, \dot{\mathrm{w}}_z) \end{pmatrix} \quad (35)$$

The references of the stored energy are determined as following (the corresponding reference of the current-error is controlled to zero, i.e., $\mathrm{w}_{z-ref} = 0$):

$$\begin{cases} \mathrm{w}_{c-ref} = \frac{1}{2} C_f \begin{pmatrix} V_{cd-ref}^2 \\ V_{cq-ref}^2 \end{pmatrix} \\ V_{cd/q-ref} = \sqrt{3/2} V_{rms} \end{cases} \quad (36)$$

Eventually, the input vector $u = [V_{d1}, V_{q1}, \dots V_{0k}, V_{dk}, V_{qk}]^T$ is to be formulated in terms of w_{c-ref}, w_{z-ref} and their corresponding derivatives. Hence, relations (34) and (35), can be written as following:

$$\begin{pmatrix} V_{d1} \\ V_{q1} \end{pmatrix} = \begin{pmatrix} \psi_{V_{d1}}(\mathrm{w}_{c-ref}, \dot{\mathrm{w}}_{c-ref}, \ddot{\mathrm{w}}_{c-ref}, \mathrm{w}_{z-ref}, \dot{\mathrm{w}}_{z-ref}) \\ \psi_{V_{q1}}(\mathrm{w}_{c-ref}, \dot{\mathrm{w}}_{c-ref}, \ddot{\mathrm{w}}_{c-ref}, \mathrm{w}_{z-ref}, \dot{\mathrm{w}}_{z-ref}) \end{pmatrix} \quad (37)$$

$$\begin{pmatrix} V_{0k} \\ V_{dk} \\ V_{qk} \end{pmatrix} = \begin{pmatrix} \psi_{V_{0k}}(\mathrm{w}_{z-ref}, \dot{\mathrm{w}}_{z-ref}) \\ \psi_{V_{d1}}(\mathrm{w}_{c-ref}, \dot{\mathrm{w}}_{c-ref}, \ddot{\mathrm{w}}_{c-ref}, \mathrm{w}_{z-ref}, \dot{\mathrm{w}}_{z-ref}) \\ \psi_{V_{q1}}(\mathrm{w}_{c-ref}, \dot{\mathrm{w}}_{c-ref}, \ddot{\mathrm{w}}_{c-ref}, \mathrm{w}_{z-ref}, \dot{\mathrm{w}}_{z-ref}) \end{pmatrix} \quad (38)$$

As implied from (26)-(38) and according to flat system formula (25), the system states and input vector verify the flatness conditions and they are found by the candidate flat output w.

C. LINEARIZATION OF CONTROL LAW

When a nonlinear system possesses the flatness property, it can be converted into a linear controllable system by feedback linearization. After linearization, stabilization, the controller becomes easier, robust to parameters variations [30]. To assure that, the trajectories w_c, w_{zk} perfectly follow their set values, i.e., w_{c-ref}, w_{zk-ref}, traditional input-output linearization is employed. Such technique introduces fictitious control variables $\beta_c = [\beta_d, \beta_q]^T$ for output energy vector w_c and $\beta_z = [\beta_{z2}, \dots, \beta_{zn}]^T$ for the current error vector w_z. For the energy output vector, derivatives of the energy components are set to:

$$\begin{cases} \ddot{\mathrm{w}}_d = \beta_d \\ \ddot{\mathrm{w}}_q = \beta_q \end{cases} \quad (39)$$

This article has been accepted for publication in a future issue of this journal, but has not been fully edited. Content may change prior to final publication. Citation information: DOI 10.1109/ACCESS.2022.3175847, IEEE Access

These controllers are obtained via (40) and (41), which permit asymptotic convergence to their respective reference trajectories.

$$\left(\ddot{\mathrm{w}}_{d-ref}-\beta_d\right)+k_{11}\left(\dot{\mathrm{w}}_{d-ref}-\dot{\mathrm{w}}_d\right)+k_{12}\left(\mathrm{w}_{d-ref}-\mathrm{w}_d\right)+ k_{13}\int\left(\mathrm{w}_{d-ref}-\mathrm{w}_d\right)d\tau=0 \quad (40)$$

$$\left(\ddot{\mathrm{w}}_{q-ref}-\beta_q\right)+k_{11}\left(\dot{\mathrm{w}}_{q-ref}-\dot{\mathrm{w}}_q\right)+k_{12}\left(\mathrm{w}_{q-ref}-\mathrm{w}_q\right)+ k_{13}\int\left(\mathrm{w}_{q-ref}-\mathrm{w}_q\right)d\tau=0 \quad (41)$$

As inferred from the control polynomial in (40) and (41) for the flat output, the constraints of the control system are then expressed as equalities. The derivative term of the control law is employed to avert introducing discontinuities. Likewise, an integral part is augmented to realize a zero steady-error and counteract other modeling mismatches. In this way, stable trajectory tracking with prescribed tracking error dynamics is guaranteed.

Fictitious control variable $\beta_{zk} = [\beta_{z0k}, \beta_{zdk}, \beta_{zqk}]^T$ for current vector error can be similarly identified as used with energy vector:

$$\begin{cases}\dot{z}_{0k}=\beta_{z0k}\\ \dot{z}_{dk}=\beta_{zdk}\forall\ k\neq i, k\in[n\neq\{i\}]\\ \dot{z}_{qk}=\beta_{zqk}\end{cases} \quad (42)$$

The second-order law is augmented with the components w_{zk} to assure that $\mathrm{w}_{zk} = [\mathrm{w}_{zok}, \mathrm{w}_{zdk}, \mathrm{w}_{zqk}]^T$ perfectly follows its planned reference w_{zk-ref}. So, the current error control law is given as following:

$$\left(\dot{\mathrm{w}}_{zk-ref}-\beta_{zk}\right)+k_{21}\left(\mathrm{w}_{zk-ref}-\mathrm{w}_{zk}\right)+k_{22}\int\left(\mathrm{w}_{zk-ref}-\mathrm{w}_{zk}\right)d\tau=0 \quad (43)$$

To express the dynamics of the flat output vector, a variable δ is introduced to simplify the model which is given by (40), (41), and (43).

$$\dddot{\delta}_{\mathrm{w}_c}+k_{11}\ddot{\delta}_{\mathrm{w}_c}+k_{12}\dot{\delta}_{\mathrm{w}_c}+k_{13}\delta_{\mathrm{w}_c}=0 \quad (44)$$

$$\ddot{\delta}_{\mathrm{w}_z}+k_{21}\dot{\delta}_{\mathrm{w}_z}+k_{22}\delta_{\mathrm{w}_z}=0 \quad (45)$$

To obtain the optimal value of the gain coefficients of (44) and (45), with better dynamics of the control system, a characteristic polynomial $p(s)$ as defined in (46) is candidated.

$$\begin{cases}p_{\mathrm{w}c}(s)=(s+p_1)\left(s^2+2\zeta_{\mathrm{w}c}\omega_{\mathrm{w}c}s+\omega_{\mathrm{w}c}^2\right)\\ p_{\mathrm{w}z}(s)=\left(s^2+2\zeta_{\mathrm{w}z}\omega_{\mathrm{w}z}s+\omega_{\mathrm{w}z}^2\right)\end{cases} \quad (46)$$

By matching (44), (45) and (46), to obtain the rewarded specified root locations, the operational behavoir of the proposed control method is set stable for: $k_{11}, k_{12}, k_{13}, k_{21}, k_{22} > 0$. Accordingly, the system dynamics will be influenced by these coefficients which are associated with control laws which listed in Table 2. The input vector $u = [V_{di}, V_{qi}, \ldots V_{0k}, V_{dk}, V_{qk}]^T$ which is described by (34) to (35) can be expressed in terms of the candidate flat output components and its derivatives following the I/O linearization technique. Then, u can be formulated by (47) and (48) in terms of w_{c-ref}, w_{zk-ref}, δ_c and δ_z:

$$\begin{pmatrix}V_{di}\\ V_{qi}\end{pmatrix}=\begin{pmatrix}\psi_{V_{d1}}(\mathrm{w}_{c-ref},\dot{\mathrm{w}}_{c-ref},\beta_c,\mathrm{w}_{z-ref},\beta_z)\\ \psi_{V_{q1}}(\mathrm{w}_{c-ref},\dot{\mathrm{w}}_{c-ref},\beta_c,\mathrm{w}_{z-ref},\beta_z)\end{pmatrix} \quad (47)$$

$$\begin{pmatrix}V_{0k}\\ V_{dk}\\ V_{qk}\end{pmatrix}=\begin{pmatrix}\psi_{V_{0k}}(\mathrm{w}_{zk-ref},\beta_z)\\ \psi_{V_{dk}}(\mathrm{w}_{c-ref},\dot{\mathrm{w}}_{c-ref},\beta_c,\mathrm{w}_{z-ref},\beta_z)\\ \psi_{V_{qk}}(\mathrm{w}_{c-ref},\dot{\mathrm{w}}_{c-ref},\beta_c,\mathrm{w}_{z-ref},\beta_z)\end{pmatrix} \quad (48)$$

D. REFERENCE TRAJECTORY PLANNING

As an advantage of the FBC, limiting the maximum current of the inductor or the input current can be readily achieved by incorporating a current limiting function in the reference of the inductor current into the controller by using a second-order filter which is introduced to the trajectories. A low-pass second-order filter is used to planify the requested path of the flat output vector $\mathrm{w} = [\mathrm{w}_c, \mathrm{w}_z]^T$ and their sub-respective components. This is to restrain power transient variation owing to variations of $V_{rms-ref}$. In addition, the trajectories follow their references without steady-state errors. Therefore, the new planned reference trajectory $\mathrm{w}_{ref-f} = [\mathrm{w}_{c_{ref-f}}, \mathrm{w}_{z_{ref-f}}]^T$ of the candidate flat output vector becomes:

$$\mathrm{w}_{c_{ref-f}}=\left(1-e^{\left(t-t_{initc}\right)/\tau_c}-\frac{\left(t-t_{initc}\right)}{\tau_c}e^{\left(t-t_{initc}\right)/\tau_c}\right)\left(\mathrm{w}_{c-ref}-\mathrm{w}_{c-init}\right)+\mathrm{w}_{c-init} \quad (49)$$

$$\mathrm{w}_{zk_{ref-f}}=\left(1-e^{\left(t-t_{initz}\right)/\tau_z}-\frac{\left(t-t_{initz}\right)}{\tau_z}e^{\left(t-t_{initz}\right)/\tau_z}\right)\left(\mathrm{w}_{zk-ref}-\mathrm{w}_{zk-init}\right)+\mathrm{w}_{zk-init} \quad (50)$$

By applying the flatness control, all constraints are reported through the candidate flat output (the energy). Also, the constraints can be given on the state and/or on the control in terms of the flat output and its derivatives. On the other hand, the presence of the observation and the current error controller system can lead to non-negligible time delays, hence, the choice of the system dynamics is crucial. The dynamics of the current error trajectories, the observer and

This article has been accepted for publication in a future issue of this journal, but has not been fully edited. Content may change prior to final publication. Citation information: DOI 10.1109/ACCESS.2022.3175847, IEEE Access

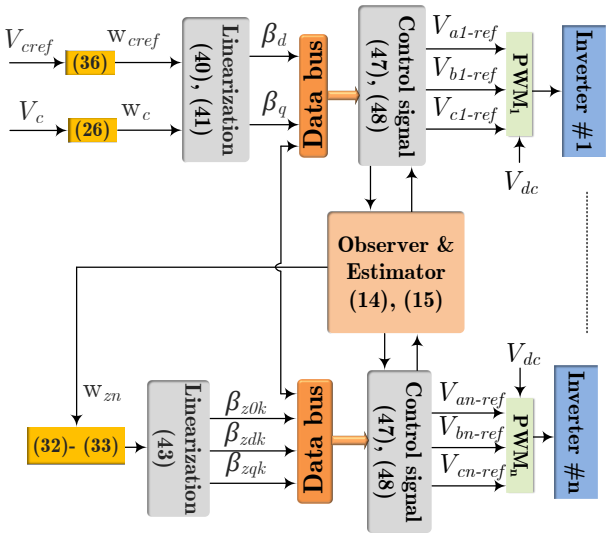

FIGURE 2: Control model of the entire parallel inverters system with the observer and estimator

TABLE 2: System Parameters

Parameter	Symbol	Value	Unit
DC input voltage	V_{in}	500	V
DC side line inductance	L	1	mH
DC side line resistance	r	0.2	Ω
DC bus capacitance	C_{dc}	800	μF
AC filter inductance	L	1	mH
AC filter resistance	r	0.2	Ω
AC Filter capacitance	C_f	40	μF
AC terminal voltage	V_t	110	V
Switching frequency	f_{sw}	15	kHz
Energy trajectory	ζ_c	0.95	-
	ω_{wc}	7000	rad/s
	p_y	5000	rad/s
Current errors trajectory	ζ_z	0.7	-
	ω_{wz}	7000	rad/s
Energy trajectory filter τ_c	ζ_c	0.95	-
	ω_c	1000	rad/s
Current errors trajectory filter τ_z	ζ_z	0.95	-
	ω_{wz}	1000	rad/s

the estimator are chosen higher than that of the energy trajectory control dynamics, as given in Table 2 to guarantee high convergence without time delay.

V. SIMULATION VERIFICATION

A detailed system is structured in Matlab environment to explore the proposed control strategy by using two-parallel inverters. The system parameters and control gains are identical to those used for the experimental investigations as listed in Table 2. Fig. 2 depicts schematic diagram of the proposed observer-based control system. Fig. 3.a illustrates response of w_{cd} and w_{cq} for the ac output filter with a step of the RMS output voltage from 80 V to 120 V at $t = 20ms$. The components w_{c0} and V_{C0} equal zero. The measured components perfectly follow their respective references. Figs. 3-b,c demonstrate response of the output three-phase voltages and their components V_{cd} and V_{cq} with the control strategy which are pure sine waves for P_L= 3 kW. The proposed FBC adjusts the output ac bus voltage to its reference set value under the normal conditions. Figs. 3-d,e show the estimated voltages for the first and the second inverters for given values for the voltages $V_{td/qn}$ and the current I_p. These voltages and current artificially represent the losses of the system. The online estimator gives the same value of the inserted voltage and current sources. Figs. 3-f,g shows the dc link voltage and the input dc current. Fig. 3.h shows the load power with a step of the RMS output voltage from 80 V to 120 V at $t = 20$ ms. Figs. 4-a,b show the response V_{c0dq} and the instantaneous voltages V_{cabc} which are set to RMS value of 110 V with a step of the load power from 3 kW to 5 kW at $t = 20$ ms. The corresponding load currents are given in Figs. 4-c,d with P_L changes from 3 kW to 5 kW. The load is set to a balanced load with a step from 3 kW to 5 kW at $t = 20$ ms as indicated in Fig. 4.e. Fig. 4.f shows the result of the total losses P_{Loss} under balanced load with a step from 3 kW to 5 kW at $t = 20$ ms and ac bus voltage equals 110 V. As the two inverters are identical, the circulating currents are absent. Furthermore, the impact of circulating currents is insignificant as the switching actions are strictly synchronous.

VI. EXPERIMENTAL VALIDATION

For further validation of the simulation tests, experimental validations are executed for 5 kW test system comprising two parallel inverters as depicted in Fig. 5. The proposed FBC method is realized by MATLAB/Simulink-RTW software. The control method is implemented owing to the dSPACE-1005 real-time control card. All the measurements are attained by digital oscilloscope: Tektronix TDS5104B and Yokogawa WT1800E. Fig. 6 shows the performance of the tested system by using the proposed FBC while initial operating point is set to V_{dc} = 500 V, V_{rms} = 110 V, $P_L = 3.2$ kW. Fig. 6.a illustrates the three-phase ac voltages and load currents for P_L= 3.2 kW and the output voltage of the ac bus V_{abc} is fixed at 110 V. The reported voltage THD is equal to 1.8%. Figs. 6-b,c show the behavior of w_{dq}, w_{dq-ref} and V_{dq}, V_{dq-ref} due to step variation of V_{cref} from 55 to 120 V while P_L =3.2 kW. As depicted, the actual values well-match their respective references. Figs. 6-d,e demonstrate waveforms of currents i_{d1}, i_{d2} and i_{q1}, i_{q2}. The proposed control method is effective where the current errors are controlled to zero. The currents i_{d1}, i_{d2}, and i_{q1}, i_{q2} are equally shared between parallel inverters owing to employed current balancing control, and the circulating current is suppressed. These results emphasize minimization of the circulating currents of the parallel inverters. In order to verify the proposed observer performances, Fig. 7.a shows the evolutions of the experimental results of i_{d1}, i_{d2} and, i_{q1}, i_{q2}, and their respective estimated values when P_L= 3.2 kW and the output ac bus voltage step from 80 V to 120 V and back to 80 V. The estimated values are identical to the

This article has been accepted for publication in a future issue of this journal, but has not been fully edited. Content may change prior to final publication. Citation information: DOI 10.1109/ACCESS.2022.3175847, IEEE Access

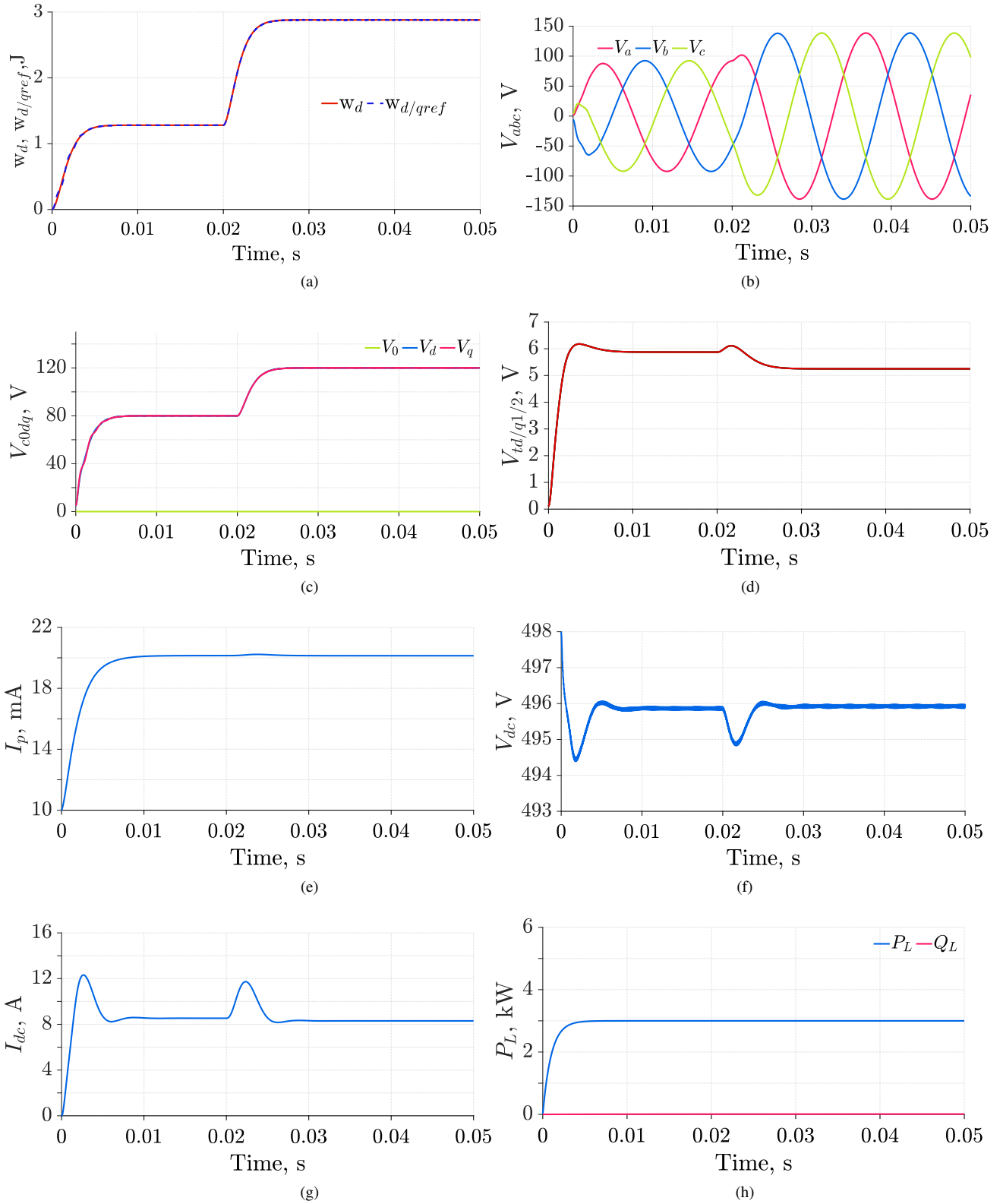

FIGURE 3: System response with FBC for a step of the RMS output voltage from 80 V to 110 V at t = 20 ms. (V_{dc} = 500 V, P_L=3 kW). (a) $w_{d/q-ref}$, $w_{d/q}$ under output ac bus voltage step from 80 V to 120 V. (b), (c) V_{abc}, V_{c-0dq} with output ac bus voltage step from 80 V to 120 V. (d) $V_{td/q-1/2}$. (e) I_p for output ac bus voltage step from 80 V to 120 V and load power of 3 kW. (f), (g) V_{dc}, I_{dc} with P_L =3 kW and output ac bus voltage step from 80 V to 120 V. (h) P_L for step of reference voltage from 80 V to 110 V.

This article has been accepted for publication in a future issue of this journal, but has not been fully edited. Content may change prior to final publication. Citation information: DOI 10.1109/ACCESS.2022.3175847, IEEE Access

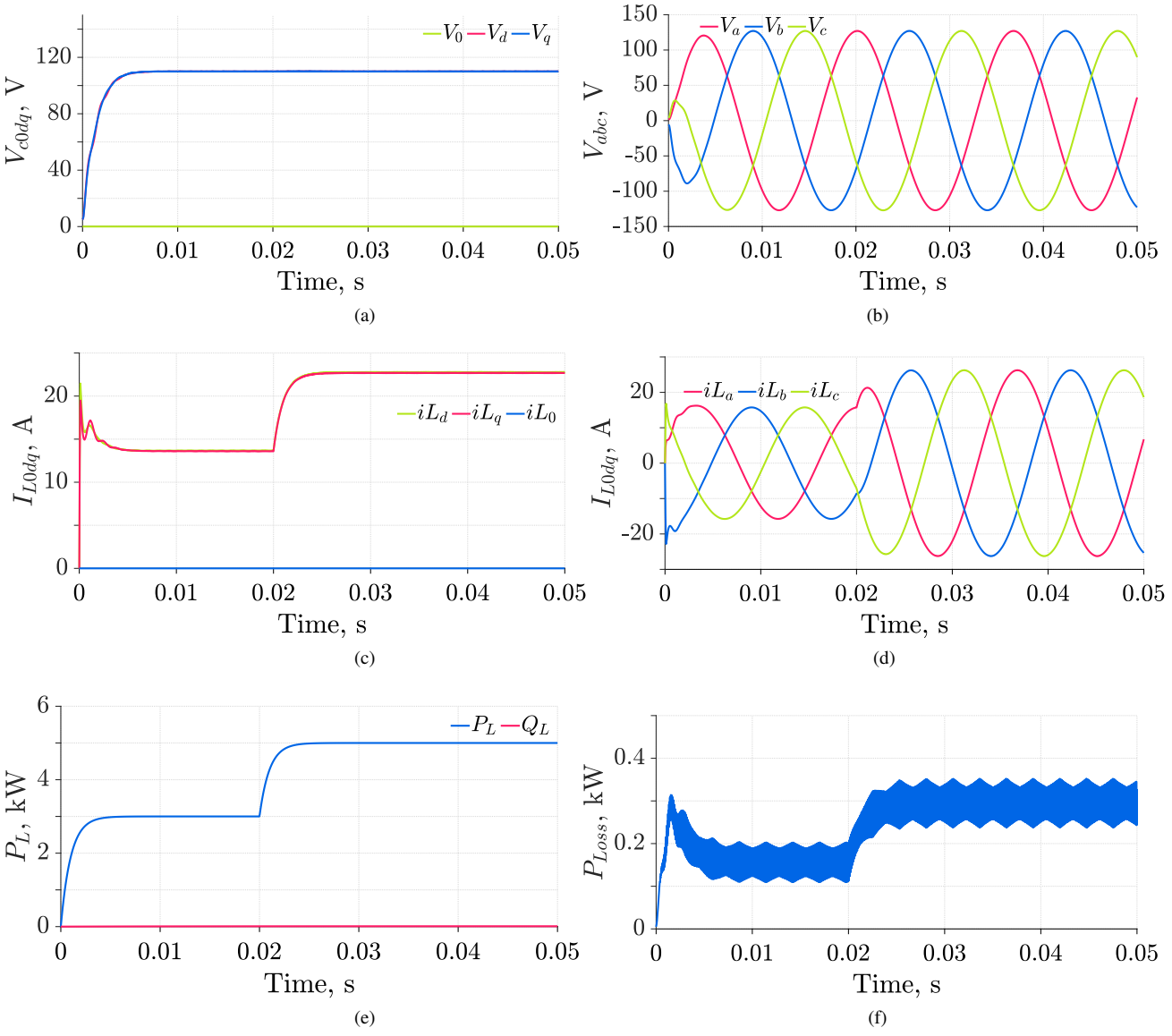

FIGURE 4: System response with FBC with load power variation from 3 kW to 5 kW at $t = 20ms$. (V_{dc} = 500 V, V_{rms} = 110 V. (a), (b) V_{c0dq}, V_{abc} for V^*_{abc} = 110 V with load change from 3 kW to 5 kW. (c), (d) i_{L0dq}, i_{Labc} for V^*_{abc} = 110 V with load variation from 3 kW to 5 kW. (e), (f) P_L, P_{Loss} for with load variation step from 3 kW to 5 kW and output ac bus voltages 110 V.

measured values.

Fig. 7.b shows the experimental results of V_{cd}, and V_{cq} when voltage changes suddenly from 80 V to 120 V and back to 80 V. Experimental results of V_{dc}, I_{dc}, and their respective estimated values under output ac bus voltage step from 80 V to 120 V and back to 80 V is depicted in Fig. 7.c. Fig. 7.d shows the experimental behaviors of $V_{td1/2}, V_{tq1/2}$ for output ac bus voltage steps from 80 V to 120 V. Fig. 7.e shows the behaviors of $Z_{d1/2}, Z_{q1/2}$, these values are forced to zero to minimize the circulating currents between the parallel inverters. These results emphasize the efficacy of the proposed current balancing scheme which ensures balanced power sharing among parallel inverters. Fig. 7.f demonstrates I_{dc} and I_P for voltage change from 55 V to 120 V.

Fig. 7.g depicts the shared power between the inverters and the corresponding losses $P_1/2$, $P_{Loss1}/2$ for each inverter under unbalanced operation cause by inserting 1.5 Ω per phase to the second inverter. As seen, P_1, P_2 are maintained balanced though the second inverter encounters higher losses. From the simulation and experimental results, the proposed FBC is effective for controlling the parallel inverters. The controlled system is robust against the uncertainties of the system parameters and the results validate the proposed estimator-based control method. The system efficiency is

This article has been accepted for publication in a future issue of this journal, but has not been fully edited. Content may change prior to final publication. Citation information: DOI 10.1109/ACCESS.2022.3175847, IEEE Access

about 94% for the assumed load. In addition, in virtue of the proposed FBC, V_{dc} and I_{dc}, I_{abcn} sensors are dispensed. It is evident that, the proposed estimators can provide information to the controller to obtain the corresponding duty cycle that maintains the output voltage equal to its reference. As seen, the number of voltage and current sensors is about 5 sensors only.

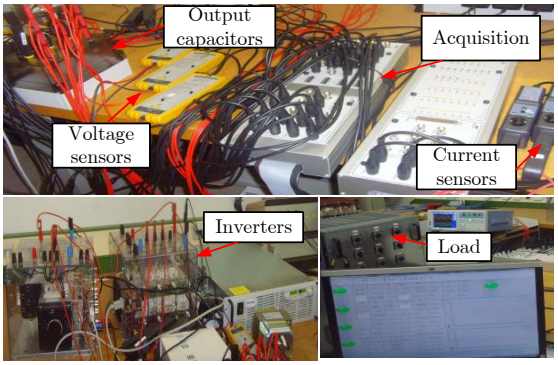

FIGURE 5: Experimental workbench of the two parallel inverters system

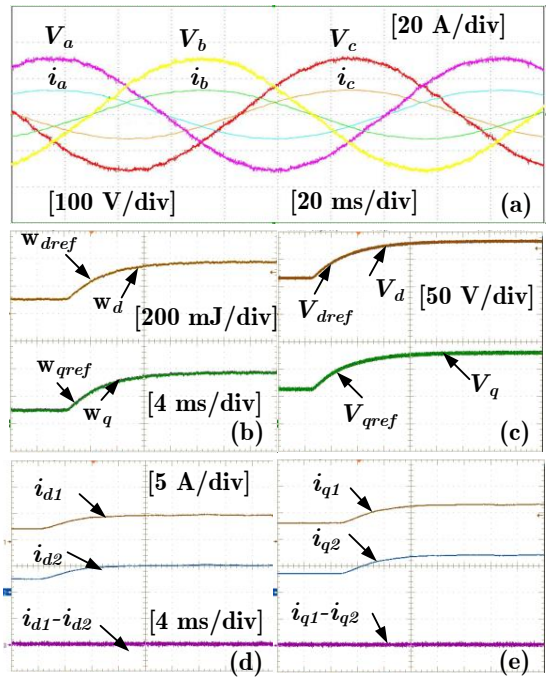

FIGURE 6: Experimental response of test system with the proposed FBC (V_{dc} =500 V, V_{rms} = 110 V, P_L = 3.2 kW). (a) V_{abc}, i_{abc} for RMS reference voltage value equal to 110 V. (b) $w_{d/q-ref}, w_{d/q}$. (c) $V_{d/q-ref}, V_{d/q}$. for step of RMS value of reference voltage from 55 V to 120 V. (d), (e) i_{d1}, i_{d2} and, i_{q1}, i_{q2} and their respective differences.

VII. CONCLUSIONS

In this paper, a sensorless flatness-based controller (FBC) for non-ideal paralleled DC-AC inverters is presented. A nonlinear online observer is suggested to estimate the line inductor currents and the dc link voltage to avoid using excessive sensors and simplify the control structure. Thereby increasing the system robustness against sudden variations of the input voltage and the load changes. A proposed method for modelling of the losses of DC/AC inverters is presented where the losses are modeled by voltage sources for each inverter and one current source. The observation system is exponentially stable, and its stability is validated by the candidate Lyapunov function which ensures that the estimation errors exponentially converge to zero. The system performance is explored by both simulation and experimental investigations, where the simulation verification is executed for two 5 kW parallel DC/AC inverters, whereas experimental validation is performed for 2 kW parallel inverters. The obtained results reveal that the control system is robust against various variations of the loads and the supply voltage.

REFERENCES

[1] S. Abulanwar, A. Ghanem, M. E. Rizk, and W. Hu, "Adaptive synergistic control strategy for a hybrid ac/dc microgrid during normal operation and contingencies," Applied Energy, vol. 304, p. 117756, 2021.

[2] Z. Wang, X. Wang, J. Cao, M. Cheng, and Y. Hu, "Direct torque control of T-NPC inverters-fed double-stator-winding PMSM drives with SVM," IEEE Trans. Power Electron., vol. 33, no. 2, pp. 1541–1553, 2017.

[3] R. Chen, J. Niu, H. Gui, Z. Zhang, F. Wang, L. M. Tolbert, D. J. Costinett, B. J. Blalock, and B. B. Choi, "Modeling, analysis, and reduction of harmonics in paralleled and interleaved three-level neutral point clamped inverters with space vector modulation," IEEE Trans. Power Electron., vol. 35, no. 4, pp. 4411–4425, 2019.

[4] A. Pal and K. Basu, "A soft-switched high-frequency link single-stage three-phase inverter for grid integration of utility scale renewables," IEEE Trans. Power Electron., vol. 34, no. 9, pp. 8513–8527, 2018.

[5] K. Wang, X. Huang, B. Fan, Q. Yang, G. Li, and M. L. Crow, "Decentralized power sharing control for parallel-connected inverters in islanded single-phase micro-grids," IEEE Trans. Smart Grid, vol. 9, no. 6, pp. 6721–6730, 2017.

[6] Q. Zhang, X. Xing, and K. Sun, "Space vector modulation method for simultaneous common mode voltage and circulating current reduction in parallel three-level inverters," IEEE Trans. Power Electron., vol. 34, no. 4, pp. 3053–3066, 2018.

[7] Q. Du, L. Gao, Q. Li, T. Li, and F. Meng, "Harmonic reduction methods at DC side of parallel-connected multipulse rectifiers: A review," IEEE Trans. Power Electron., vol. 36, no. 3, pp. 2768–2782, 2020.

[8] L. Yang, H. Zhao, S. Wang, and Y. Zhi, "Common-mode EMI noise analysis and reduction for AC–DC–AC systems with paralleled power modules," IEEE Trans. Power Electron., vol. 35, no. 7, pp. 6989–7000, 2019.

[9] Y. Qi, Y. Tang, K. R. R. Potti, and K. Rajashekara, "Robust power sharing control for parallel three-phase inverters against voltage measurement errors," IEEE Trans. Power Electron., vol. 35, no. 12, pp. 13 590–13 601, 2020.

[10] X. Meng, Z. Liu, H. Zheng, and J. Liu, "A universal controller under different operating states for parallel inverters with seamless transfer capability," IEEE Trans. Power Electron., vol. 35, no. 9, pp. 9794–9812, 2020.

This article has been accepted for publication in a future issue of this journal, but has not been fully edited. Content may change prior to final publication. Citation information: DOI 10.1109/ACCESS.2022.3175847, IEEE Access

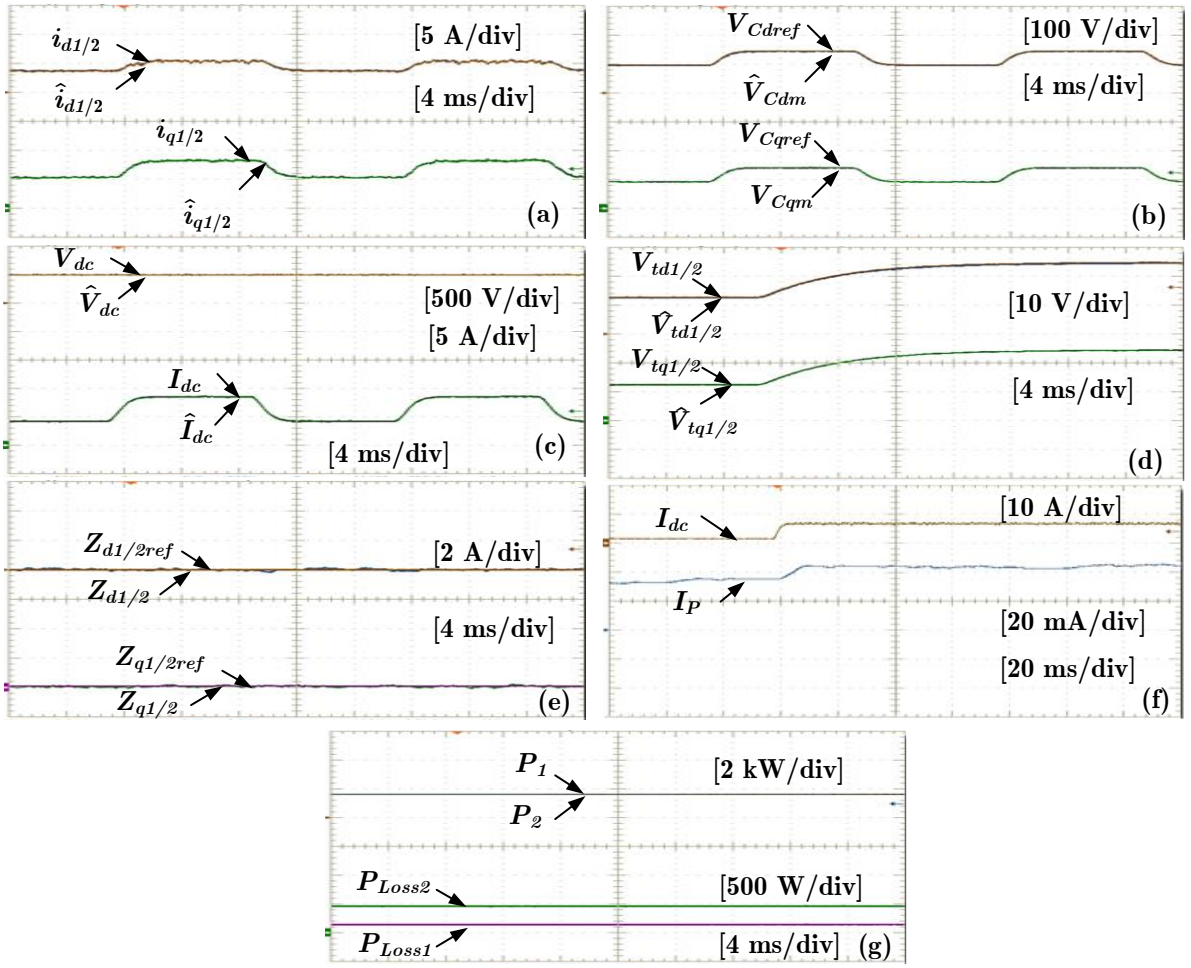

FIGURE 7: Experimental response of test system with the proposed FBC (V_{dc} =500 V, V_{rms} = 110 V, P_L = 3.2 kW). (a) $i_{d1/2}$, $\hat{i}_{d1}$, $i_{q1/2}$, $\hat{i}_{q1}$ (b) $V_{cd/q-ref}$, $V_{cd/qm}$ with voltage changes from 80 V to 120 V and back to 80 V. (c) V_{dc}, $\hat{V}_{dc}$, I_{dc}, $\hat{I}_{dc}$ with voltage changes from 80 V to 120 V and back to 80 V. (d) $V_{tdq1/2}$, $\hat{V}_{tdq1/2}$ with voltage step from 80 V to 120 V. (e) $Z_{dq1/2-ref}$, $Z_{dq1/2}$. (f) I_{dc}, I_P with voltage step from 55 V to 120 V. (g) $P_{1/2}$, P_{Loss}

.

[11] W. Wu, L. Zhou, Y. Chen, A. Luo, Y. Dong, X. Zhou, Q. Xu, L. Yang, and J. M. Guerrero, "Sequence-impedance-based stability comparison between VSGs and traditional grid-connected inverters," IEEE Trans. Power Electron., vol. 34, no. 1, pp. 46–52, 2018.

[12] S. Sikkabut, P. Mungporn, B. Yodwong, C. Ekkaravarodome, B. Nahid-Mobarakeh, S. Pierfederici, B. Davat, and P. Thounthong, "Comparative study of control approaches of li-ion battery/supercapacitor storage devices for fuel cell power plant," in 2015 International Conference on Clean Electrical Power (ICCEP). IEEE, 2015, pp. 647–652.

[13] M. Phattanasak, R. Gavagsaz-Ghoachani, J.-P. Martin, B. Nahid-Mobarakeh, S. Pierfederici, and B. Davat, "Comparison of two nonlinear control strategies for a hybrid source system using an isolated three-port bidirectional DC-DC converter," in 2011 IEEE Vehicle Power and Propulsion Conference. IEEE, 2011, pp. 1–6.

[14] L. Zhang and G.-H. Yang, "Observer-based adaptive decentralized fault-tolerant control of nonlinear large-scale systems with sensor and actuator faults," IEEE Trans. Ind. Electron., vol. 66, no. 10, pp. 8019–8029, 2018.

[15] N. N. N. Nam, N.-D. Nguyen, C. Yoon, M. Choi, and Y. I. Lee, "Voltage sensorless model predictive control for a grid-connected inverter with LCL filter," IEEE Trans. Ind. Electron., 2021.

[16] Y. Zhang, Z. Wang, J. Jiao, and J. Liu, "Grid-voltage sensorless model predictive control of three-phase PWM rectifier under unbalanced and distorted grid voltages," IEEE Trans. Power Electron., vol. 35, no. 8, pp. 8663–8672, 2019.

[17] L. Ding, Y. W. Li, and N. R. Zargari, "Discrete-time SMO sensorless control of current source converter-fed PMSM drives with low switching frequency," IEEE Trans. Ind. Electron., vol. 68, no. 3, pp. 2120–2129, 2020.

[18] X. Zhou, Y. Zhou, C. Peng, F. Zeng, and X. Song, "Sensorless BLDC motor commutation point detection and phase deviation correction method," IEEE Trans. Power Electron., vol. 34, no. 6, pp. 5880–5892, 2018.

[19] A. Khodaparast, M. J. Hassani, E. Azimi, M. E. Adabi, J. Adabi, and E. Pouresmaeil, "Circuit configuration and modulation of a seven-level switched-capacitor inverter," IEEE Trans. Power Electron., vol. 36, no. 6, pp. 7087–7096, 2020.

[20] S.-S. Huang, Y. Konishi, Z.-Z. Yang, and M.-J. Hsieh, "Observer-based capacitor current sensorless control applied to a single-phase inverter system with seamless transfer," IEEE Trans. Power Electron., vol. 34, no. 3, pp. 2819–2828, 2018.

[21] D. Liang, J. Li, R. Qu, and W. Kong, "Adaptive second-order sliding-mode

observer for PMSM sensorless control considering VSI nonlinearity," IEEE Trans. Power Electron., vol. 33, no. 10, pp. 8994–9004, 2017.

[22] Y. Wang, Y. Xu, and J. Zou, "Sliding-mode sensorless control of PMSM with inverter nonlinearity compensation," IEEE Trans. Power Electron., vol. 34, no. 10, pp. 10 206–10 220, 2019.

[23] X. Wu, S. Huang, K. Liu, K. Lu, Y. Hu, W. Pan, and X. Peng, "Enhanced position sensorless control using bilinear recursive least squares adaptive filter for interior permanent magnet synchronous motor," IEEE Trans. Power Electron., vol. 35, no. 1, pp. 681–698, 2019.

[24] A. Devanshu, M. Singh, and N. Kumar, "An improved nonlinear flux observer based sensorless FOC IM drive with adaptive predictive current control," IEEE Trans. Power Electron., vol. 35, no. 1, pp. 652–666, 2019.

[25] F. Xiong, J. Wu, Z. Liu, and L. Hao, "Current sensorless control for dual active bridge DC–DC converter with estimated load-current feedforward," IEEE Trans. Power Electron., vol. 33, no. 4, pp. 3552–3566, 2017.

[26] J. He and X. Zhang, "A modified lyapunov-based control scheme for a three-phase ups with an optimal third-order load current observer," in 2019 IEEE 10th International Symposium on Power Electron. for Distributed Generation Systems (PEDG). IEEE, 2019, pp. 233–236.

[27] H. Yang, Y. Zhang, J. Liang, J. Gao, P. D. Walker, and N. Zhang, "Sliding-mode observer based voltage-sensorless model predictive power control of PWM rectifier under unbalanced grid conditions," IEEE Trans. Ind. Electron., vol. 65, no. 7, pp. 5550–5560, 2017.

[28] A. Djerioui, A. Houari, A. Saim, M. Aït-Ahmed, S. Pierfederici, M. F. Benkhoris, M. Machmoum, and M. Ghanes, "Flatness-based grey wolf control for load voltage unbalance mitigation in three-phase four-leg voltage source inverters," IEEE Trans. Ind Appl., vol. 56, no. 2, pp. 1869–1881, 2019.

[29] P. Thounthong, S. Sikkabut, N. Poonnoy, P. Mungporn, B. Yodwong, P. Kumam, N. Bizon, B. Nahid-Mobarakeh, and S. Pierfederici, "Nonlinear differential flatness-based speed/torque control with state-observers of permanent magnet synchronous motor drives," IEEE Trans. Ind Appl., vol. 54, no. 3, pp. 2874–2884, 2018.

[30] A. Shahin, H. Moussa, I. Forrisi, J.-P. Martin, B. Nahid-Mobarakeh, and S. Pierfederici, "Reliability improvement approach based on flatness control of parallel-connected inverters," IEEE Trans. Power Electron., vol. 32, no. 1, pp. 681–692, 2016.

[31] M. Fliess, J. Lévine, P. Martin, and P. Rouchon, "Flatness and defect of non-linear systems: introductory theory and examples," International journal of control, vol. 61, no. 6, pp. 1327–1361, 1995.

[32] A. Shahin, J.-P. Martin, and S. Pierfederici, "Zero-sequence current based diagnostic method for open-switch fault detection in parallel inverters system," IEEE Trans. Power Electron., vol. 34, no. 4, pp. 3750–3764, 2018.

[33] M. Zandi, A. Payman, J.-P. Martin, S. Pierfederici, B. Davat, and F. Meibody-Tabar, "Energy management of a fuel cell/supercapacitor/battery power source for electric vehicular applications," IEEE Trans. Veh. Technol, vol. 60, no. 2, pp. 433–443, 2010.

[34] A. Shahin, M. Hinaje, J.-P. Martin, S. Pierfederici, S. Raël, and B. Davat, "High voltage ratio DC–DC converter for fuel-cell applications," IEEE Trans. Ind. Electron., vol. 57, no. 12, pp. 3944–3955, 2010.

[35] M. Pahlevaninezhad, P. Das, J. Drobnik, P. K. Jain, and A. Bakhshai, "A new control approach based on the differential flatness theory for an AC/DC converter used in electric vehicles," IEEE Trans. Power Electron., vol. 27, no. 4, pp. 2085–2103, 2011.

[36] P. Thounthong, "Control of a three-level boost converter based on a differential flatness approach for fuel cell vehicle applications," IEEE Trans. Veh. Technol, vol. 61, no. 3, pp. 1467–1472, 2012.

[37] H.-C. Chen, C.-Y. Lu, and U. S. Rout, "Decoupled master-slave current balancing control for three-phase interleaved boost converters," IEEE Trans. Power Electron., vol. 33, no. 5, pp. 3683–3687, 2017.

[38] M. Borrega, L. Marroyo, R. Gonzalez, J. Balda, and J. L. Agorreta, "Modeling and control of a master–slave PV inverter with N-paralleled inverters and three-phase three-limb inductors," IEEE Trans. Power Electron., vol. 28, no. 6, pp. 2842–2855, 2012.

[39] J. R. García-Sánchez, E. Hernandez-Marquez, J. Ramírez-Morales, M. Marciano-Melchor, M. Marcelino-Aranda, H. Taud, and R. Silva-Ortigoza, "A robust differential flatness-based tracking control for the "mimo dc/dc boost converter–inverter–dc motor" system: Experimental results," IEEE Access, vol. 7, pp. 84 497–84 505, 2019.

[40] P. Mercorelli, "Combining flatness based feedforward action with a fractional pi regulator to control the intake valve engine," in 2017 18th International Carpathian Control Conference (ICCC). IEEE, 2017, pp. 456–461.

[41] M. He, Q. Ge, and W. Liu, "Some problems analysis of observability and observable degree for complex stochastic systems," in 2018 3rd International Conference on Advanced Robotics and Mechatronics (ICARM). IEEE, 2018, pp. 863–868.

[42] P. Zhuo, Q. Ge, T. Shao, Y. Wang, and L. Bai, "Observable degree analysis using unscented information filter for nonlinear estimation systems," in 2015 10th International Conference on Information, Communications and Signal Processing (ICICS). IEEE, 2015, pp. 1–6.

[43] M. He, Q. Ge, J. Ma, and T. Chen, "Observable degree analysis of kalman filter with correlated noises," in 2017 2nd International Conference on Advanced Robotics and Mechatronics (ICARM). IEEE, 2017, pp. 517–522.

[44] M. Khlif and M. Shawky, "Observability checking to enhance diagnosis of real time electronic systems," in 2008 12th IEEE/ACM International Symposium on Distributed Simulation and Real-Time Applications. IEEE, 2008, pp. 69–74.

[45] N. Ayllon, A. Anakabe, J. M. Collantes, G. Soubercaze-Pun, and S. Forestier, "Sensitivity enhancement in pole-zero identification based stability analysis of microwave circuits," in 2008 Workshop on Integrated Nonlinear Microwave and Millimetre-Wave Circuits. IEEE, 2008, pp. 75–78.

[46] A. Anakabe, N. Ayllon, J. Collantes, A. Mallet, G. Soubercaze-Pun, and K. Narendra, "Automatic pole-zero identification for multivariable large-signal stability analysis of rf and microwave circuits," in The 40th European Microwave Conference. IEEE, 2010, pp. 477–480.

[47] M. Tarokh, "Frequency-domain criteria for controllability and observability of multivariable systems," in 1986 American Control Conference. IEEE, 1986, pp. 782–787.

[48] H. Renaudineau, J.-P. Martin, B. Nahid-Mobarakeh, and S. Pierfederici, "Dc–dc converters dynamic modeling with state observer-based parameter estimation," IEEE Trans. Power Electron., vol. 30, no. 6, pp. 3356–3363, 2014.

[49] R. Gavagsaz-Ghoachani, M. Phattanasak, J.-P. Martin, B. Nahid-Mobarakeh, S. Pierfederici, and P. Riedinger, "Observer and lyapunov-based control for switching power converters with lc input filter," IEEE Trans. Power Electron., vol. 34, no. 7, pp. 7053–7066, 2018.

AHMED SHAHIN (M'08 - SM'15) received the B.Sc. and M.Sc. degrees in Electrical Engineering from Mansoura University, Mansoura, Egypt respectively in 2000 and 2004, and the Ph.D. degree in electrical engineering from the Ecole Nationale Supérieure d'electricité et de Mécanique, Université de Lorraine, Nancy, France, in 2011. Since 2012, he has been engaged as Associate Professor, Faculty of Engineering, Mansoura University, Mansoura Egypt. His current research interests include the renewable energy systems, modeling, optimization methods, which are oriented to the power management, control, and fault diagnosis of the photovoltaic systems and fault tolerant in the power electronic systems. In recent years, his research interests include the areas of the electrical vehicles, distributed generation systems and multisource microgrids.

This article has been accepted for publication in a future issue of this journal, but has not been fully edited. Content may change prior to final publication. Citation information: DOI 10.1109/ACCESS.2022.3175847, IEEE Access

SAYED ABULANWAR (S'12-M'16) received the B.Sc. and M.Sc. degrees in Electrical Engineering, Mansoura University, Egypt, in 2005 and 2010, respectively, and the Ph.D. degree from Energy Technology Department, Aalborg University, Denmark, in 2016. He is currently an Associate Professor, Faculty of Engineering, Mansoura University, Egypt. He is a Associate Editor, IET Renewable Power Generation and Guest Editor, IET Renewable Power Generation for Special issue: Applications of Artificial Intelligence in Renewable Energy Systems. His research includes hybrid AC/DC Microgrids, protection of AC and DC systems, wind energy conversion systems, transients in power systems and grid-connected converters.

ABDELHADY GHANEM (M'18) received the B.Sc., M.Sc., and Ph.D. degrees, all in Electrical Engineering, from Mansoura University, Mansoura, Egypt, in 2006, 2011, and 2017, respectively. Since 2006, he has been employed by the Electrical Engineering Department at Mansoura University, where he is now an Assistant Professor. He joined University of Nottingham, Nottingham, U.K., as an Occasional PhD Student (Joint Supervision Scheme between Mansoura University and University of Nottingham) from February 2015 to May 2017. His research interests include electrical systems modelling, renewable power generation, power system analysis and control, grid connected power electronics converters, and stability analysis.

MOHAMMAD E. M. RIZK (M'19) received the B.Sc. and M.Sc. degrees in Electrical Engineering from Mansoura University, Mansoura, Egypt in 2007 and 2011 respectively, and the D.Sc. degree from Aalto University, Espoo, Finland, in 2016. He joined Aalto University as a postdoctoral researcher at the Department of Electrical Engineering and Automation in 2017. Currently, he is Associate Professor of Electrical Engineering at Mansoura University. His research interests include power system transients, lightning overvoltages in power systems and transient electromagnetic fields.

FUJIN DENG (Senior Member, IEEE) received the B.Eng. degree in Electrical Engineering from China University of Mining and Technology, Jiangsu, China, in 2005, the M.Sc. Degree in Electrical Engineering from Shanghai Jiao Tong University, Shanghai, China, in 2008, and the Ph. D. degree in Energy Technology from the Department of Energy Technology, Aalborg University, Aalborg, Denmark, in 2012.

He joined the Southeast University in 2017 as a Professor in the School of Electrical Engineering, Southeast University, Nanjing, China. From 2013 to 2015 and from 2015 to 2017, he was a Postdoctoral Researcher and an Assistant Professor, respectively, in the Department of Energy Technology, Aalborg University, Aalborg, Denmark. His main research interests include wind power generation, multilevel converters, high-voltage direct-current technology, DC grid and offshore wind farm-power systems dynamics.

SERGE PIERFEDERICI received the engineer degree from the 'Ecole Nationale Supérieure d'Electricité et Mécanique', Nancy-Lorraine, France, in 1994, and the Ph.D. degree in electrical engineering from the Institut National Polytechnique de Lorraine in 1998. Since 2009, he is Full Professor at the Lorrain University and member of the LEMTA. He is the authors or co-authors or more than 100 international peer reviewed journals and has been the recipient of several IEEE awards. His research interests include the stability study of distributed power systems, the modelling and control of power electronic systems and since recent years the distributed control of multi sources multi carrier microgrids.

ISLAM ISMAEL received the B.Sc., M.Sc. and Ph.D degrees in electrical engineering from Mansoura University, Mansoura, Egypt, in 2006, 2011 and 2017 respectively. He is currently an Assistant Professor of Electrical Engineering with Mansoura University. His research interests include, microgrids optimization and grid-connected converters.